Pure and Applied Geophysics

Validation and Verification of Tsunami Numerical Models

C. E. Synolakis,[1] E. N. Bernard,[2] V. V. Titov,[3] U. Kânoğlu,[4] and F. I. González[2]

Abstract—In the aftermath of the 26 December, 2004 tsunami, several quantitative predictions of inundation for historic events were presented at international meetings differing substantially from the corresponding well-established paleotsunami measurements. These significant differences attracted press attention, reducing the credibility of all inundation modeling efforts. Without exception, the predictions were made using models that had not been benchmarked. Since an increasing number of nations are now developing tsunami mitigation plans, it is essential that all numerical models used in emergency planning be subjected to validation—the process of ensuring that the model accurately solves the parent equations of motion—and verification—the process of ensuring that the model represents geophysical reality. Here, we discuss analytical, laboratory, and field benchmark tests with which tsunami numerical models can be validated and verified. This is a continuous process; even *proven* models must be subjected to additional testing as new knowledge and data are acquired. To date, only a few existing numerical models have met current standards, and these models remain the only choice for use for real-world forecasts, whether short-term or long-term. Short-term forecasts involve data assimilation to improve forecast system robustness and this requires additional benchmarks, also discussed here. This painstaking process may appear onerous, but it is the only defensible methodology when human lives are at stake. Model standards and procedures as described here have been adopted for implementation in the U.S. tsunami forecasting system under development by the National Oceanic and Atmospheric Administration, they are being adopted by the Nuclear Regulatory Commission of the U.S. and by the appropriate subcommittees of the Intergovernmental Oceanographic Commission of UNESCO.

Key words: Tsunami, benchmarked tsunami numerical models, validated and verified tsunami numerical models.

1. Introduction

Following the Indian Ocean tsunami of 26 December, 2004, there has been substantial interest in developing tsunami mitigation plans for tsunami prone regions worldwide (Synolakis and Bernard, 2006). While UNESCO has been attempting to coordinate capacity building in tsunami hazards reduction around the world, several national agencies have been making exceptional progress towards being tsunami-ready.

[1] Viterbi School of Engineering, University of Southern California, Los Angeles, CA 90089, USA.

[2] NOAA/Pacific Marine Environmental Laboratory, Seattle, WA 98115, USA.

[3] NOAA/Pacific Marine Environmental Laboratory, Seattle, WA 98115, USA and Joint Institute for the Study of the Atmosphere and Ocean (JISAO), University of Washington, Seattle, WA 98195, USA.

[4] Department of Engineering Sciences, Middle East Technical University, 06531 Ankara, Turkey.

The National Oceanic and Atmospheric Administration (NOAA) is the federal agency charged with mitigating tsunami hazards in the United States. Tsunami models are prominent in two components of the NOAA strategy: Short-term forecast products in support of Tsunami Warning Centers (TWCs) operated by the National Weather Service and long-term forecast products such as inundation maps for hazard assessment and planning by Member States of the National Tsunami Hazard Mitigation Program (NTHMP). The NTHMP was formed through a directive of the U.S. Senate Appropriations Committee in 1994 to develop a plan for a tsunami warning system that reduces the risk to coastal residents. After the Indian Ocean tsunami, the U.S. expanded the role of NTHMP to serve as the organizational framework to implement the recommendations of the NATIONAL SCIENCE and TECHNOLOGY COUNCIL (2005).

One of the recommendations was to "Develop standardized and coordinated tsunami hazard and risk assessments for all coastal regions of the U.S. and its territories." Standards for modeling tools do not currently exist, yet an increased number of states either are developing or will need to develop tsunami mitigation plans. There is risk that forecast products may be produced with older or untested methodologies. This is a worldwide problem, as the Intergovernmental Oceanographic Commission (IOC) of UNESCO has found out in its efforts to help member nations develop tsunami hazard maps. Unrealistic estimates can be costly both in terms of lives lost, or in unnecessary evacuations that sometimes put lives at risk and reduce the credibility of the world system. Standards are urgently needed to ensure a minimum level of quality and reliability for real-time forecasting and inundation mapping products. Further, unrealistic estimates can lead to panic. Examples include the 30 m runup estimates for Cascadia tsunamis (THE SEATTLE TIMES, 2005; NEW SCIENTIST, 2005; ASSOCIATED PRESS, 2005) and large runup estimates for islands in the Eastern Mediterranean in 2007 (ETHNOS, 2007); in both instances, an inordinate effort took place to restore common sense.

In the past ten years, the process of model validation and verification has shown that coastal effects of tsunamis can be described by a set of depth-averaged hydrostatic equations of motion, also known as the shallow-water wave (SW) equations. Comparisons with both large-scale laboratory data and field data have demonstrated a compelling and not always expected capability to describe complex evolution phenomena, and to estimate the maximum runup and inundation, over wide ranges of tsunami waves. In the current state of knowledge, the main uncertainty arises from the ambiguities of the initial condition, assuming the solution methodology solves the equations of motion satisfactorily. The increasing deployment of Deep-ocean Assessment and Reporting of Tsunamis (DART) buoys—tsunameters or tsunamographs—that monitor tsunami evolution in the deep ocean, allows for real-time updates of the characteristics of the source and thus leads to better definition of the initial conditions, at least for tectonic tsunamis (SATAKE *et al.*, 2007). Realistic initial data as input in benchmarked computational tools lead to focused and reliable forecasts.

While equation solvers of higher-than-the-SW approximations of the parent Navier–Stokes equations now exist, they are presently too computationally intensive for

inundation mapping or operational forecasting, and are generally used for free-surface flows of very limited geographical extent. These models remain largely unvalidated over wide ranges of tsunami events and in fact many of them work only in one propagation direction. Yet, the rapid development of packaged numerical modeling tools facilitates their application by untrained users.

In the next section, we discuss model evaluation with state-of-the-art benchmark tests for validating and verifying computational tools for predicting the coastal effect of tsunamis. Then, we recommend standards and guidelines for operational codes used for inundation mapping and tsunami forecasting.

2. Model Evaluation Standards

Tsunami models have evolved in the last two decades through careful and explicit validation/verification by comparing their predictions with benchmark analytical solutions, laboratory experiments, and field measurements. While there is in principle no assurance that a numerical code that has performed well in all benchmark tests will always produce realistic inundation predictions, validated/verified codes largely reduce the level of uncertainty in their results to the uncertainty in the geophysical initial conditions. Furthermore, when coupled with real-time free-field tsunami measurements from tsunameters, validated/verified codes are the only choice for realistic forecasting of inundation.

Here we develop recommendations for national agencies approval of modeling tools, their further development, and their transfer to operations. These steps can be classified into four categories: basic hydrodynamic considerations, benchmarking, scientific evaluations, and operational evaluations.

2.1. Basic Hydrodynamic Considerations

Mass conservation: While the equation of conservation of mass is solved in all numerical computations of water-wave motions, cumulative numerical approximations can sometimes produce results that violate the principle. This is particularly true when the model employs friction factors or smoothing to stabilize inundation computations. For a closed domain within reflective boundaries, conservation of mass can be checked by calculating the water volume at the beginning and end of the computation, derived upon integration of the disturbed water surface $\eta(x, y, t)$ over the entire solution domain up to the maximum extend of inundation. The integral of the entire flow depth $h(x, y, t)$, where $h(x, y, t) = \eta(x, y, t) + d(x, y, t)$ and $d(x, y, t)$ is the undisturbed water depth, should not be used; typically, $\eta \ll d$ offshore, and integrating h will tend to mask errors. For a domain with open or absorbing boundaries, the net volume flux across each such boundary must be considered in the estimate of total displaced volume. Numerical errors in such computations can be highly additive, and mass invariably might not be conserved in long numerical

computations. Nonetheless, the initial total displaced volume should agree with the displaced volume at the end of the computation within a prespecified margin of error. If the difference is not acceptable, then the code numerics must be examined for errors or inadequacies, and/or the grid must be readjusted. Improvements can usually be achieved with a few changes in grid size(s) and time step. Obviously the process must be shown to converge to increasingly smaller mass losses.

Convergence: Extreme runup/rundown locations are optimally suited for checking convergence of the numerical code used to a certain asymptotic limit, presumably the actual solution of the equations solved. A graph needs to be prepared presenting the variation of the calculated runup/rundown (ordinate) with the step size (abscissa). As the step size is reduced, the numerical predictions should be seen to converge to a certain value, with further reductions in step size not appreciably changing the results. One excellent example is given in PEDERSEN (2008).

2.2. Benchmark Solutions

Benchmarking of numerical models can be classified into analytical, laboratory, and field benchmarking. Some of the benchmarks we will describe here have been used in the 1995 and 2004 Long-Wave Runup Models Workshops in Friday Harbor, Washington (YEH *et al.*, 1996) and Catalina, California (LIU *et al.*, 2008), respectively. More detailed descriptions of these benchmarks are given in SYNOLAKIS *et al.* (2007).

2.2.1 Analytical benchmarking. The real usefulness of analytical calculation is its identification of the dependence of desired results (such as runup) on the problem parameters (such as offshore wave height, beach slope, depth variation). Numerical solutions will invariably produce more accurate specific predictions, but will rarely provide useful information about the problem scaling, unless numerical computations are repeated *ad nauseam*. Comparisons with exact solutions can identify systematic errors and are thus useful in validating the complex numerical methods used in realistic applications.

Here, we present analytical solutions to certain common 1+1 (one directional and time) propagation problems. The results are derived for idealized initial waveforms often used in tsunami engineering to describe the leading wave of a tsunami. Generalization to more realistic spectral distributions of geophysical tsunamis is trivial, given that results are shown in closed-form integrals.

It is important to note that validation should always take place with non-periodic waves. During runup, individual monochromatic waves reflect with slope-dependent phase shifts (SYNOLAKIS, 1986). Whereas a particular code may model a periodic wave well, it may not model superposition equally well. This was a problem of earlier SW computations that did not account for reflection. While their predictions for the Carrier–Greenspan (CARRIER and GREENSPAN, 1958) sinusoids appeared satisfactory, they exhibited significant errors when modeling solitary waves or N-waves.
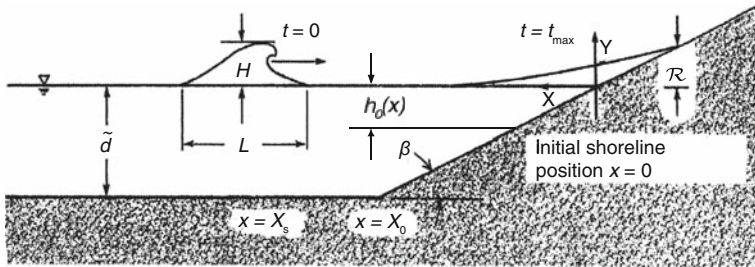
Figure 1
Definition sketch for a canonical consideration.

Linear solutions on a simple beach: We consider a solitary and N-wave propagation first over the constant-depth region then sloping beach—canonical problem (Fig. 1). The topography is described by $h_0(x) = x \tan\beta$ when $x \le X_0$ and $h_0(x) = 1$ when $x \ge X_0$ where $X_0 = \cot\beta$. The origin of the coordinate system is at the initial position of the shoreline and x increases seaward. Even though dimensionless variables are not preferred in numerical calculations and engineering practice, in analytical solutions they have distinct advantages as everything scales simply with an offshore characteristic depth or a characteristic length. Here dimensionless variables are introduced as: $x = \tilde{x}/\tilde{d}$, $(h, \eta, h_0, \mathcal{R}) = (\tilde{h}, \tilde{\eta}, \tilde{h}_0, \tilde{\mathcal{R}})/\tilde{d}$, $u = \tilde{u}/\sqrt{\tilde{g}\tilde{d}}$, and $t = \tilde{t}/\sqrt{\tilde{d}/\tilde{g}}$ provided the depth $\tilde{d}$ of the constant-depth region is chosen as the characteristic scale. Quantities with tilde are dimensional and η is the amplitude, u is the depth-averaged horizontal velocity, h_0 is the undisturbed water depth, and $\tilde{g}$ is the gravitational acceleration.

Consider a tsunami evolution problem described by the $1 + 1$ nonlinear shallow-water wave (NSW) equations:

$$h_t + (u\,h)_x = 0, \quad u_t + uu_x + \eta_x = 0, \tag{1}$$

with $h(x, t) = \eta(x, t) + h_0(x)$. Neglecting nonlinear terms, through elementary manipulations, (1) reduces to an equation $\eta_{tt} - (\eta_x\,h_0)_x = 0$ known as the linear shallow-water wave (LSW) equation. SYNOLAKIS (1986, 1987) matched the linear theory solution at the constant-depth region with the linear solution over the sloping beach as derived by KELLER and KELLER (1964) to determine the solution for the wave height $\eta(x, t)$ over the sloping beach,

$$\eta(x, t) = 2 \int\limits_{-\infty}^{+\infty} \Phi(\omega) \frac{J_0(2\omega\sqrt{xX_0})e^{-i\omega(X_0+t)}}{J_0(2X_0\omega) - iJ_1(2X_0\omega)}\, d\omega. \tag{2}$$

Here, $\Phi(\omega)$ is the spectrum of the incoming wave offshore. This solution is only valid when $0 \le x \le X_0$; LSW equation does not reduce to Bessel's equation when $x < 0$. Notice that the integral (2) can be evaluated with standard numerical methods; however, the advantage of this form is that it allows calculation of the solution for many physically

realistic tsunami waveforms simply by using the $\Phi(\omega)$ of the incoming wave in (2), hopefully known at some offshore location.

Solitary wave evolution and runup: An initial solitary wave centered offshore at $x = X_s$ has the surface profile, $\eta(x, t = 0) = H \operatorname{sech}^2 \gamma(x - X_s)$ where $\gamma = \sqrt{3H/4}$ and H is the dimensionless wave height, i.e., $H = \widetilde{H}/\widetilde{d}$. Upon substituting its spectrum in equation (2), SYNOLAKIS (1991) showed that the maximum local value of the wave amplitude $\eta_{\max}$ is given explicitly by $\eta_{\max}/H = (X_0/x)^{1/4} = (1/h_0)^{1/4}$, an amplitude variation usually referred to as *Green's law*. The region over which this amplitude variation applies is the region of gradual shoaling; the region of rapid shoaling is often identified with the Boussinesq result, i.e., $\eta_{\max} \sim h_0$. The fact that both evolution laws may coexist was first identified by SHUTO (1973). SYNOLAKIS and SKJELBREIA (1993) also present results which show that Green's law type evolution is valid over a wide range of slopes and for finite-amplitude waves at least in the region of gradual shoaling.

In the LSW theory, the shoreline does not move beyond $x = 0$. The maximum value of $R(t) = \eta(0, t)$ is the maximum runup $\mathcal{R}$, arguably the most important parameter in the long-wave runup problem, and it is the maximum vertical excursion of the shoreline. The result (2) can be readily applied to derive the maximum runup of a solitary wave climbing up a sloping beach. Per SYNOLAKIS (1986), the integral (2) with the solitary wave spectrum $\Phi(\omega)$ can be reduced into a Laurent series using contour integration. The series can be simplified further by using the asymptotic form for large arguments of the modified Bessel functions, making it possible to obtain its extremum, leading to the following expression for the maximum runup $\mathcal{R}$:

$$\mathcal{R} = 2.831 \sqrt{\cot\beta}\, H^{5/4}. \tag{3}$$

This result is formally correct when $\sqrt{H} \gg 0.288 \tan\beta$, the assumption implied when using the asymptotic form of the Bessel functions. The asymptotic result (3) is valid for waves that do not break during runup. Equation (3) was derived by SYNOLAKIS (1986) and has since been referred to as *the runup law* and shown in Figure 2. As will be apparent in later sections, this methodology is quite powerful to find the maximum runup and it allows calculation of the runup of other waveforms such as N-waves, not to mention the runup of waves evolving over piecewise-linear bathymetries.

N-wave runup: Most tsunami eyewitness accounts suggest that tsunamis are N-wave like, i.e., they are dipolar, which means they appear as a combination of a depression and an elevation wave, and frequently as a series of N-waves, sometimes known as double N-waves. Until the late 1990s, the solitary wave model was used exclusively to evaluate the runup of tsunamis. Even though it was suspected that the leading tsunami wave might be a depression wave (MEI, 1983), before 1992, these waves were believed to be hydrodynamically unstable; the crest was assumed to quickly overtake the trough. The N-wave model was motivated by observations from a series of nearshore-triggered tsunamis starting in 1992 (TADEPALLI and SYNOLAKIS, 1994; SYNOLAKIS and OKAL, 2005), all of which produced tsunami waves which caused nearby shorelines to first recede before advancing. The most
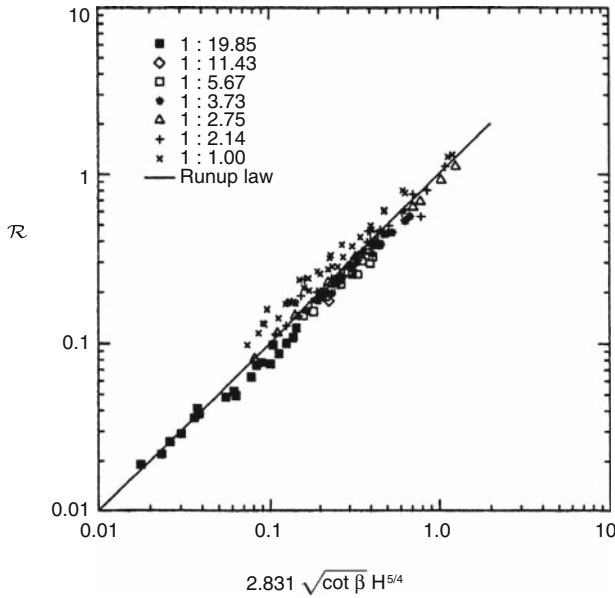
Figure 2

Laboratory data for maximum runup of nonbreaking waves climbing up different beach slopes: 1:19.85 (SYNOLAKIS, 1986); 1:11.43, 1:5.67, 1:3.73, 1:2.14, and 1:1.00 (HALL and WATTS, 1953); 1:2.75 (PEDERSEN and GJEVIK, 1983). The solid line represents the runup law (3).

spectacular account was during the 9 October, 1995 Manzanillo, Mexico earthquake. Minutes after the earthquake, one eyewitness saw the shoreline retreat beyond a rock outcrop which was normally submerged in over 4 m depth and at a distance of about 400 m from the shoreline (BORRERO et al., 1997), suggesting a leading-depression N-wave (LDN). Before the megatsunami of 26 December, 2004, this had been the only photographic evidence of LDN. Recall that the megatsunami manifested itself first with a rapid withdrawal in most locales east of the rupture zone, and as a leading-elevation N-wave (LEN) west of it (SYNOLAKIS and KONG, 2006).

To reflect the fact that tsunamigenic faulting in subduction zones is associated with both vertical uplift and subsidence of the sea bottom, TADEPALLI and SYNOLAKIS (1994, 1996) conjectured that all tsunami waves at generation have an N-wave or dipole shape. TADEPALLI and SYNOLAKIS (1996) proposed a general function as a unified model for both nearshore and farfield tsunamis as generalized N-waves, i.e., a wave propagates with the trough first is referred to as an LDN and the crest arrives first is referred to as an LEN. For a special class of N-waves with elevation and depression waves of the same height H, referred to as isosceles N-waves, $\eta(x,0) = \mathcal{H}\,\text{sech}^2[\gamma(x - X_N)]\tanh[\gamma(x - X_N)]$ with $\mathcal{H} = \frac{3\sqrt{3}H}{2}$ and $\gamma = \frac{3}{2}\sqrt{\sqrt{\frac{3}{4}H}}$, using contour integration and the same asymptotic approximation methodology as used in the solitary wave results, TADEPALLI and SYNOLAKIS (1994) showed that

$$\mathcal{R}_{LEN} = 3.86\sqrt{\cot\beta}\, H^{5/4}. \qquad (4)$$

Because of the symmetry of the profile, this is also the minimum rundown of an isosceles LDN. TADEPALLI and SYNOLAKIS (1994) also showed that the normalized maximum runup of nonbreaking isosceles LEN is smaller than the runup of isosceles LDN, and that both are higher than the runup of a solitary wave with the same wave height. The latter became known as *the N-wave effect* (Fig. 3).

Nonlinear solutions on a simple beach: Calculation of the nonlinear evolution of a wave over a sloping beach is theoretically and numerically challenging due to the moving boundary singularity. Yet, it is important to have a good estimate of the shoreline velocity and associated runup/rundown motion, since they are crucial for the planning of coastal flooding and of coastal structures. To solve the nonlinear set (1) for the single sloping beach case, $h_0(x) = x$ (Fig. 4), CARRIER and GREENSPAN (1958) used the characteristic length $\tilde{l}$ as a scaling parameter and introduced the dimensionless variables as: $x = \tilde{x}/\tilde{l}$, $(h, \eta, h_0, \mathcal{R}) = (\tilde{h}, \tilde{\eta}, \tilde{h}_0, \tilde{\mathcal{R}})/(\tilde{l}\tan\beta)$, $u = \tilde{u}/\sqrt{g\tilde{l}\tan\beta}$, and $t = \tilde{t}/\sqrt{\tilde{l}/(\tilde{g}\tan\beta)}$. CARRIER and GREENSPAN (1958) defined a hodograph transformation known as Carrier–Greenspan transformation
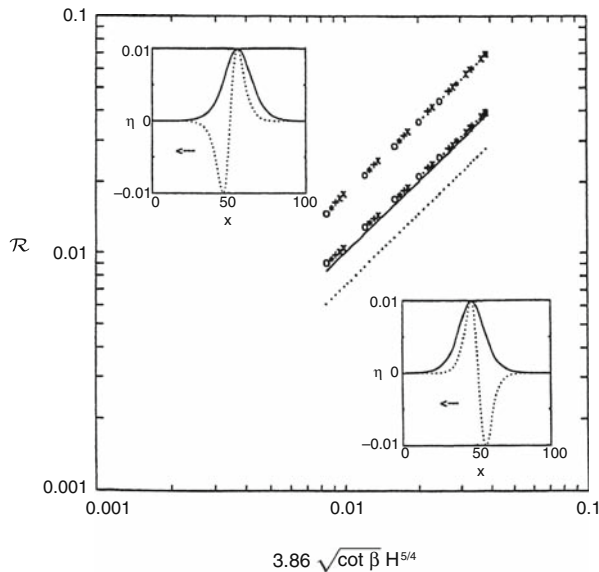

Figure 3

Maximum runup of isosceles N-waves and solitary wave. The top and lower set of points are results for the maximum runup of leading-depression and -elevation isosceles N-waves, respectively. The dotted line represents the runup of solitary wave (3). The upper and lower insets compare a solitary wave profile to a leading-depression and -elevation isosceles N-waves, respectively. After TADEPALLI and SYNOLAKIS (1994).
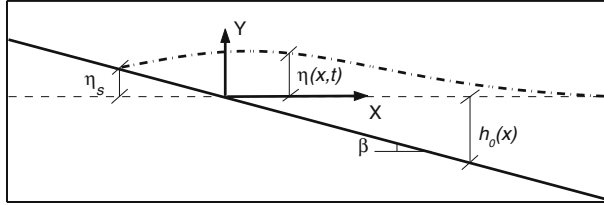
Figure 4
Definition sketch for an initial value problem.

$$x = \frac{\sigma^2}{16} - \eta, \quad t = u - \frac{\lambda}{2}, \quad \eta = \frac{\psi_\lambda}{4} - \frac{u^2}{2}, \quad u = \frac{\psi_\sigma}{\sigma}, \tag{5}$$

thus reducing the NSW equations to a single second-order linear equation:

$$(\sigma\psi_\sigma)_\sigma - \sigma\psi_{\lambda\lambda} = 0. \tag{6}$$

Here $\psi(\sigma, \lambda)$ is a Carrier–Greenspan potential. Notice the conservation of difficulty. Instead of having to solve the coupled nonlinear set (1), one now has to solve a linear equation (6), however the transformation equations (5) which relate the transformed variables to the physical variables are nonlinear, coupled, and implicit. Yet, a redeeming feature is that in the hodograph plane, i.e., in the (σ, λ)-space, the instantaneous shoreline is always at $\sigma = 0$. This allows for direct analytical solutions without the complications of the moving shoreline boundary.

In general, it is quite difficult to specify boundary or initial data for the nonlinear problem in the physical (x, t)-space coordinates without making restrictive assumptions; a boundary condition requires specification of $(X_0, \forall t)$ while an initial condition requires specification at $(\forall x, t_0)$. Even when boundary or initial conditions are available in the (x, t)-space, the process of deriving the equivalent conditions in the (σ, λ)-space is not trivial. These difficulties have restricted the use of Carrier–Greenspan transformation, and this is why they are discussed here again, in an attempt to demystify them.

Boundary value problem (BVP) for the constant depth/beach topography: Using the solution (2) of the equivalent linear problem, at the seaward boundary of the beach, i.e., at $x = X_0 = \cot\beta$ corresponding to $\sigma = \sigma_0 = 4$ based on characteristic depth scale, SYNOLAKIS (1986, 1987) was able to show that the Carrier–Greenspan potential is given by

$$\psi_b(\sigma, \lambda) = -\frac{16i}{X_0} \int_{-\infty}^{+\infty} \frac{\Phi(\kappa)}{\kappa} \frac{J_0(\sigma\kappa X_0/2)e^{-i\kappa X_0\left(1-\frac{\lambda}{2}\right)}}{J_0(2\kappa X_0) - iJ_1(2\kappa X_0)} \, d\kappa. \tag{7}$$

Note that the hodograph transformation includes $\cot\beta$ as coefficient because the scaling used in SYNOLAKIS (1986, 1987), i.e., $x = \cot\beta\left(\frac{\sigma^2}{16} - \eta\right)$ and $t = \cot\beta\left(u - \frac{\lambda}{2}\right)$. Then the amplitude $\eta(x, t)$ can be calculated directly from equation (5), so comparisons with numerical simulations for any given $\Phi(\kappa)$ is possible and straightforward. One example of the application of the BVP solution of SYNOLAKIS (1986, 1987) is given in Figure 5.
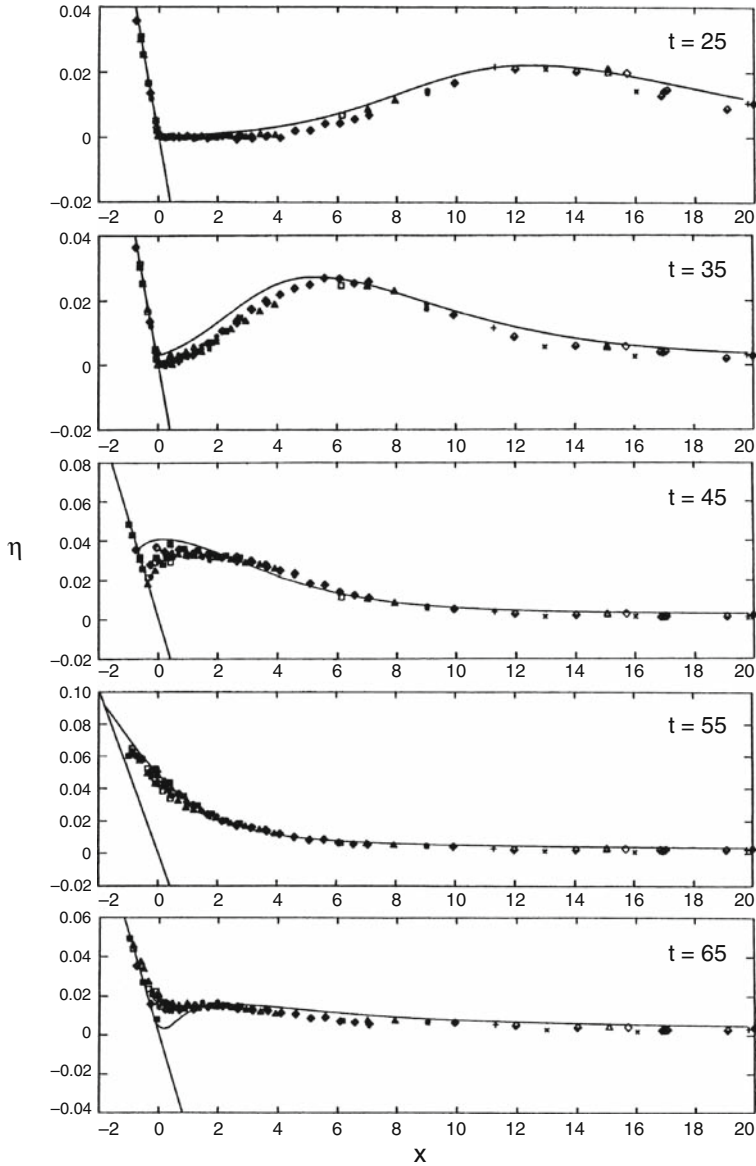
Figure 5

Time evolution of a $\tilde{H}/\tilde{d} = 0.0185$ solitary wave up a 1:19.85 beach (Fig. 1). While the markers show different realizations of the same experiment, the solid lines show boundary value problem solution of the nonlinear shallow-water wave equations. Refer to SYNOLAKIS (1986, 1987) for details.

Initial value problem (IVP) for a sloping beach: For the initial condition where $\Psi(\sigma) = u_\lambda(\sigma, 0) = 4\eta_\sigma(\sigma, 0)/\sigma$, CARRIER and GREENSPAN (1958) presented the following potential in the transform space,

$$\psi_i(\sigma, \lambda) = -\int_0^\infty \int_0^\infty \frac{1}{\omega} \xi^2 \Psi(\xi) J_0(\omega\sigma) J_1(\omega\xi) \sin(\omega\lambda) \, \mathrm{d}\omega\mathrm{d}\xi. \tag{8}$$

Note that a characteristic length scale is used to define dimensionless variables. Kânoğlu (2004) proposed that the difficulty of deriving an initial condition in the (σ, λ)-space is overcome by simply using the linearized form of the hodograph transformation for a spatial variable in the definition of initial condition. Once an IVP is specified in the (x, t)-space as $\eta(x, 0)$, the linearized hodograph transformation $x \cong \frac{\sigma^2}{16}$ is used directly to define the initial waveform in the (σ, λ)-space, $\eta\left(\frac{\sigma^2}{16}, 0\right)$. Thus $\Psi(\sigma) = 4\eta_\sigma\left(\frac{\sigma^2}{16}, 0\right)/\sigma$ is found, and $\psi_i(\sigma, \lambda)$ follows directly through a simple integration.

Once $\psi_i(\sigma, \lambda)$ is known, one can investigate any realistic initial waveform such as Gaussian and N-wave shapes as employed in CARRIER *et al.* (2003). While Kânoğlu (2004) does not consider waves with initial velocities, later, Kânoğlu and Synolakis (2006) solved a more general initial condition, i.e., initial wave with velocity.

Since it is important for coastal planning, simple expressions for shoreline runup/rundown motion and velocity are useful. Considering that the shoreline corresponds to $\sigma = 0$ in the (σ, λ)-space, the runup/rundown motion can be evaluated. Here, note that the mathematical singularity of the $u = \psi_\sigma/\sigma$, i.e., $J_1(\omega\sigma)/\sigma$, at the shoreline ($\sigma = 0$) is removed with the consideration of the $\lim_{\sigma\to 0}[J_1(\omega\sigma)/\sigma] = \frac{\omega}{2}$ (SYNOLAKIS, 1986; Kânoğlu, 2004). An example is provided in Figure 6 for IVP (Kânoğlu, 2004).

Solitary wave on a composite beach: 1+1 models that perform well with the single beach analytical solutions must still be tested with the composite beach geometry, for which an analytical solution exists, with solitary waves as inputs. Most topographies of engineering interest can be approximated by piecewise-linear segments allowing the use of LSW equation to determine approximate analytical results for the wave runup in closed form. In principle, fairly complex bathymetries can be represented through a combination of positively/negatively sloping and constant-depth segments. Solutions of the LSW equation at each segment can be matched analytically at the transition points between the
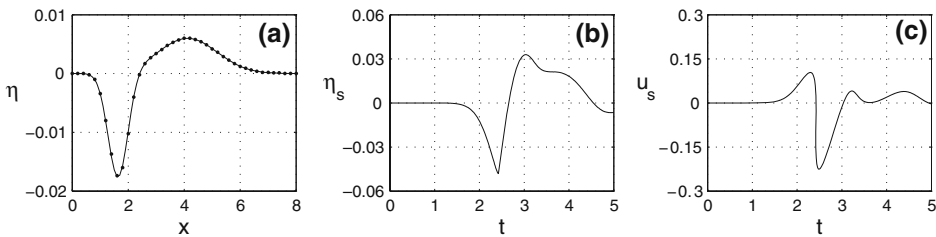

Figure 6

Initial value problem solution of the nonlinear shallow-water wave equations. (a) The leading-depression initial waveform presented by CARRIER *et al.* (2003), $\eta(x, 0) = H_1 \exp\left(-c_1(x - x_1)^2\right) - H_2 \exp\left(-c_2(x - x_2)^2\right)$ with $H_1 = 0.006$, $c_1 = 0.4444$, $x_1 = 4.1209$, $H_2 = 0.018$, $c_2 = 4.0$, and $x_2 = 1.6384$ (solid line) compared with the one resulting from approximation (dots), using the linearized form of the transformation for the spatial variable, (b) shoreline position, and (c) shoreline velocity. After Kânoğlu (2004).
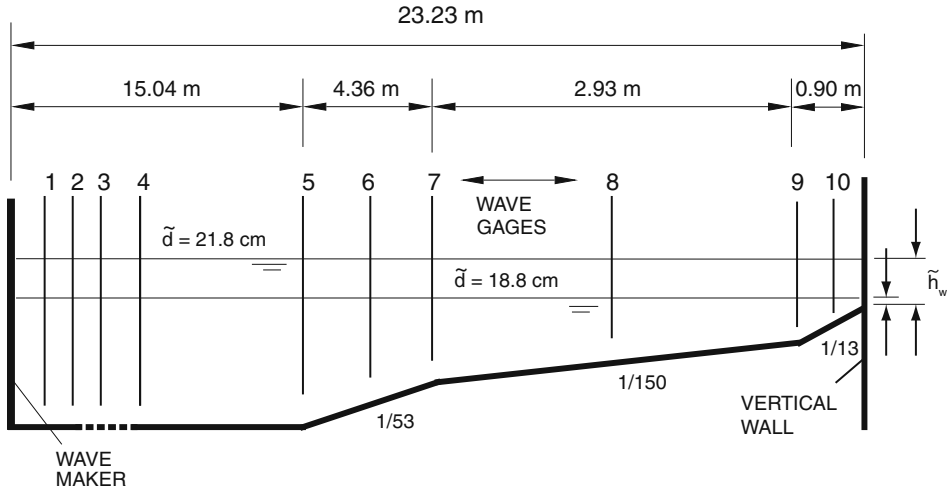
Figure 7

Definition sketch for the Revere Beach topography. $h_w = \widetilde{h}_w/\widetilde{d}$ is the water depth at the foot of the seawall, i.e., there were $\widetilde{h}_w = 1.7$ cm and 4.7 cm depths at the seawall when $\widetilde{d} = 18.8$ cm and 21.8 cm, respectively. Not to scale.

segments, and then the overall amplification factor and reflected waves can be determined, analytically. As an example, KÂNOĞLU and SYNOLAKIS (1998) considered three sloping segments and a vertical wall at the shoreline, as in Revere Beach in Massachusetts (Fig. 7). They were able to show that the maximum runup of solitary waves with maximum wave height H can be calculated analytically and is given by the runup law,

$$\mathcal{R} = 2h_w^{-1/4}H. \qquad (9)$$

The runup law above suggests that the maximum runup only depends on the depth at the seawall h_w fronting the beach, and it does not depend on any of the three slopes in front of the seawall. Laboratory data exist for this topography and the runup law (9) predicts the nonbreaking data surprisingly well (Fig. 8). The laboratory data are discussed briefly in section 2.2.2 and in greater detail in YEH *et al.* (1996), KÂNOĞLU (1998), and KÂNOĞLU and SYNOLAKIS (1998).

Subaerial landslide on a simple beach: Inundation computations are exceedingly difficult when the beach is deforming during a subaerial landslide. LIU *et al.* (2003) considered tsunami generation by a moving slide on a uniformly sloping beach, using the forced LSW equation of TUCK and HWANG (1972), and were able to derive an exact solution. Let $\widetilde{\delta}$ and $\widetilde{L}$ be the maximum vertical thickness of the sliding mass and its horizontal length respectively, and $\mu = \widetilde{\delta}/\widetilde{L}$. Tilde representing dimensional quantities, LIU *et al.* (2003) normalized the forced LSW equation with $(\eta, h_0, \mathcal{R}) = (\widetilde{\eta}, \widetilde{h}_0, \widetilde{\mathcal{R}})/\widetilde{\delta}$, $x = \widetilde{x}/\widetilde{L}$, and $t = \widetilde{t}/\left(\sqrt{\widetilde{\delta}/\widetilde{g}}/\mu\right)$, i.e., $\eta_{tt} - (\tan\beta/\mu)(\eta_x x)_x = h_{0,tt}$ where $h_0(x, t)$ is the time-dependent
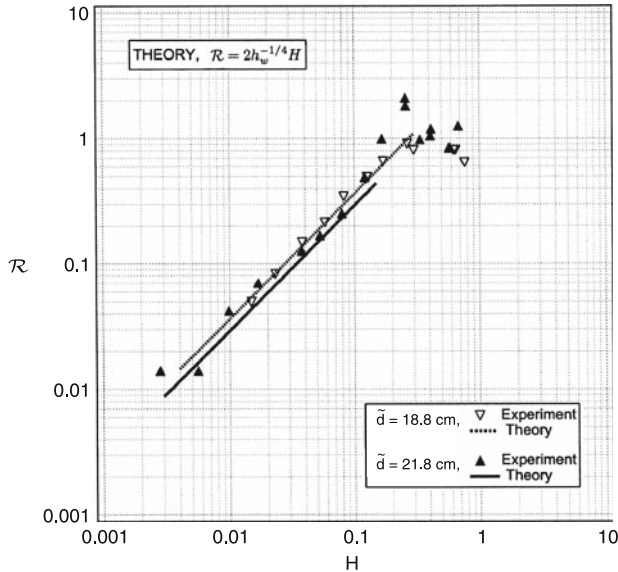
Figure 8

Comparison of the maximum runup values for the linear analytical solution (9) and the laboratory results for two different depths, i.e., $\tilde{d} = 18.8$ cm and 21.8 cm. h_w is the nondimensional depth at the toe of the seawall, and it varies with $\tilde{d}$. After KÂNOĞLU and SYNOLAKIS (1998).

perturbation of the sea floor with respect to the uniformly sloping beach. The focus in their analysis is on thin slides where $\mu = \tilde{\delta}/\tilde{L} \ll 1$.

Consider a translating Gaussian-shaped mass, initially at the shoreline, given by $h_0(x, t) = \exp[-(\xi - t)^2]$ with $\xi = 2\sqrt{\mu x/\tan\beta}$. Once in motion, the mass moves at constant acceleration. The free surface wave height is given by

$$\eta(\xi, t) = \int_0^\infty J_0(\rho\xi)\rho\left[a(\rho)\cos(\rho t) + \frac{1}{\rho}b(\rho)\sin(\rho t)\right]d\rho + \frac{1}{3}(h_0 - \xi\, h_{0,\xi}), \qquad (10)$$

where $a(\rho)$ and $b(\rho)$ can be determined by the initial conditions, i.e., unperturbed water surface and zero velocity initially. Details can be found in LIU *et al*. (2003), nevertheless it is clear that once the seafloor motion is specified, the wave height can be calculated explicitly. Figure 9 shows one example of the solution. Comparisons of the maximum runup estimates of this solution with a nonlinear numerical computation are shown in Figure 10, as an example of the validation process.

2.2.2 Laboratory benchmarking. Long before the availability of numerical codes, physical models at small scale had been used to visualize wave phenomena in the laboratory and then predictions were scaled to the prototype. Even today, when designing harbors, laboratory experiments—scale model tests—are used to confirm different flow details and validate the numerical model used in the analysis.
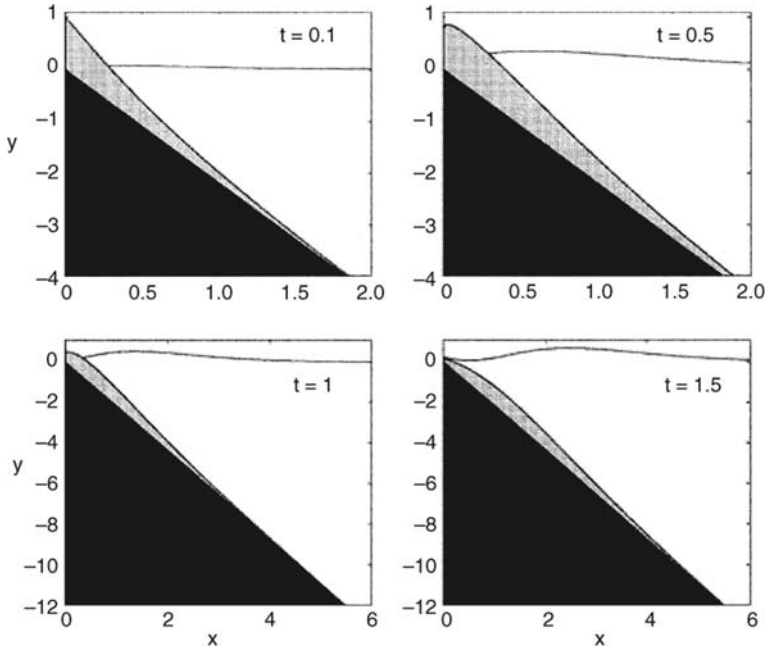
Figure 9

Spatial snapshots of the analytical solution at four different times for a beach slope, $\beta = 5°$, and landslide aspect ratio, $\mu = 0.05$ ($\tan\beta/\mu = 1.75$). The slide mass is indicated by the light shaded area, the solid beach slope by the black region, and η by the solid line (LIU *et al.*, 2003).
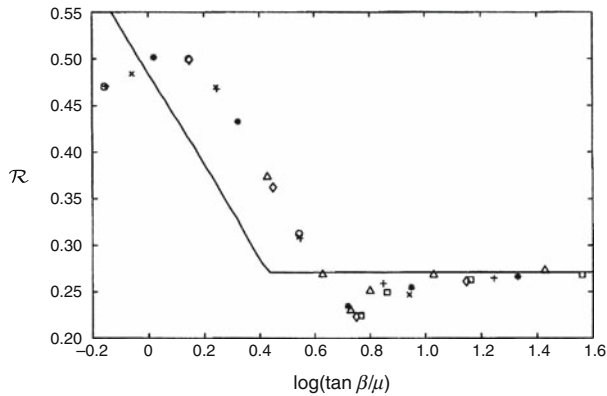

Figure 10

Maximum runup as a function of $\log(\tan\beta/\mu)$. The analytical solutions are shown by the solid line, and the various symbols are from nonlinear shallow-water wave simulations of LIU *et al.* (2003), corresponding to different slopes ranging from 2° to 20°.

Numerical codes developed in the last decade that consistently produce predictions in excellent agreement with measurements from small-scale laboratory experiments have been shown to also model geophysical-scale tsunamis well. For example, a numerical code that adequately models the inundation observed in a 1-m-deep laboratory model is also expected to compute the inundation in a 1-km-deep geophysical basin, as the grid sizes are adjusted accordingly and in relationship to the scale of the problem. While scale laboratory models, in general, do not have bottom friction characteristics similar to real ocean floors or sandy beaches, this has proven not to be a severe limitation for validation of numerical models. It is a problem when the laboratory results are used for designing prototype structures by themselves and without the benefit of numerical models. For example, sediment transport cannot be extrapolated from the laboratory to geophysical scales because the dynamics of sand grain motions do not scale proportionally to the geometric scales of the model, and it is otherwise impossible to achieve dynamic similarity.

The results from five laboratory experiments are described as laboratory benchmarking: Solitary wave experiments on a 1:19.85 sloping beach (SYNOLAKIS, 1986, 1987), on a composite beach (KÂNOĞLU, 1998; KÂNOĞLU and SYNOLAKIS, 1998), and on a conical island (BRIGGS *et al.*, 1995; LIU *et al.*, 1995; KÂNOĞLU, 1998; KÂNOĞLU and SYNOLAKIS, 1998); tsunami runup onto a complex three-dimensional beach (TAKAHASHI, 1996); and tsunami generation and runup due to a three-dimensional landslide (LIU *et al.*, 2005).

For the solitary wave experiments, the initial location, X_s in the analysis changes with different wave heights; solitary waves of different heights have different effective *wavelengths*. A measure of the *wavelength* of a solitary wave is the distance between the point x_f on the front and the point x_t on the tail where the local height is 1% of the maximum, i.e., $\eta(x_f, t = 0) = \eta(x_t, t = 0) = (\widetilde{H}/\widetilde{d})/100$. The distance X_s is at an offshore location where only 5% of the solitary wave is already over the beach, so that scaling can work. Therefore, in the laboratory experiments initial wave heights are identified at a point $X_s = X_0 + (1/\gamma) \operatorname{arccosh}\sqrt{20}$ with $\gamma = \sqrt{3(\widetilde{H}/\widetilde{d})/4}$. In the laboratory, even idealized solitary waveforms dissipate. If the wave height is measured far offshore and used as an initial condition for non-dissipative numerical models, the comparisons will be less meaningful, as the solitary wave will slightly change as it propagates towards the beach in the laboratory. By keeping the same relative offshore distance for defining the initial condition, meaningful comparisons are assured.

Solitary wave on a simple beach: Given that a small number of 2+1 wave basin laboratory measurements exists, 1+1 versions of the 2+1 numerical models should be first tested with 1+1 directional laboratory models. The solitary wave experiments on the canonical model should be used first (SYNOLAKIS, 1987). In this set of experiments, the 36.60-m-long, 0.38-m-wide, and 0.61-m-deep California Institute of Technology, Pasadena, California wave tank was used with water at varying depths. The tank is described by HAMMACK (1972), GORING (1978), and SYNOLAKIS (1986). A ramp with a slope of 1:19.85 was installed at one end of the tank to model the bathymetry of the

canonical problem of a constant-depth region adjoining a sloping beach. The toe of the ramp was 14.95 m distant from the rest position of the piston used to generate waves.

A total exceeding 40 experiments with solitary waves running up the sloping beach was performed, with depths ranging from 6.25–38.32 cm. Solitary waves are uniquely defined by their maximum height $\widetilde{H}$ to depth $\widetilde{d}$ ratio and the depth, i.e., $\widetilde{H}/\widetilde{d}$ and $\widetilde{d}$ are sufficient to specify the wave. $\widetilde{H}/\widetilde{d}$ ranged from 0.021 to 0.626. Breaking occurs when $\widetilde{H}/\widetilde{d} > 0.045$, for this particular beach.

This set of laboratory data has been used extensively for code validation: Refer to SYNOLAKIS (1987), ZELT (1991), TITOV and SYNOLAKIS (1995; 1997; 1998), TITOV and GONZÁLEZ (1997), GRILLI *et al.* (1997), LI and RAICHLEN (2000; 2001; 2002). In particular, the data sets for the $\widetilde{H}/\widetilde{d} = 0.0185$ (Fig. 5) nonbreaking and $\widetilde{H}/\widetilde{d} = 0.3$ (Fig. 11) breaking solitary waves seem the most often used and most appropriate for code validation.

Solitary wave on a composite beach: 1+1 models that perform well with the solitary wave on simple beach experiments must still be tested with the Revere Beach composite beach geometry. Revere Beach is located approximately 6 miles northeast of Boston in the City of Revere, Massachusetts. To address beach erosion and severe flooding problems, a physical model was constructed at the Coastal Engineering Laboratory of the U.S. Army Corps of Engineers, Vicksburg, Mississippi facility, earlier known as Coastal Engineering Research Center. The model beach consists of three piecewise-linear slopes of 1:53, 1:150, and 1:13 from seaward to shoreward with a vertical wall at the shoreline (Fig. 7). In the laboratory, to evaluate the overtopping of the seawall, the wavemaker was located at 23.22 m and tests were done at two depths, 18.8 cm and 21.8 cm.

In the experiments, solitary waves of different heights $\widetilde{H}/\widetilde{d}$ were generated at the location X_s for the reason explained. In terms of specific measurements, time histories of the water surface elevations exist at the locations X_s, midway in each sloping segment, and at the transition points. One example of the time histories of water surface elevations is given in Figure 12 and compared with the analytical solution of KÂNOĞLU and SYNOLAKIS (1998). A comparison of numerical results with a laboratory case near the breaking limit offshore will ensure that the code remains stable, even for extreme waves. The runup variation for solitary waves striking the vertical wall was also determined. The maximum runup values on the vertical wall were measured visually and are presented in Figure 8 for the whole experimental parameter range.

Solitary wave on a conical island: 2+1 dimensional calculations should be tested with the conical island geometry. Motivated by the catastrophe in Babi Island, Indonesia (YEH *et al.*, 1994), during the 1992 Flores Island tsunami, large-scale laboratory experiments were performed at the Coastal Engineering Research Center, Vicksburg, Mississippi, in a 30-m-wide, 25-m-long, and 60-cm-deep wave basin (Fig. 13). An initial solitary wave-like profile was created in the basin by a Directional Spectral Wave Generator (DSWG) located at $\widetilde{x} = 12.96$ m from the center of the island. The particular 27.42-m-long DSWG consisted of sixty 46 cm × 76 cm individual paddles, each driven independently. Allowing generation of waves with different crest lengths.
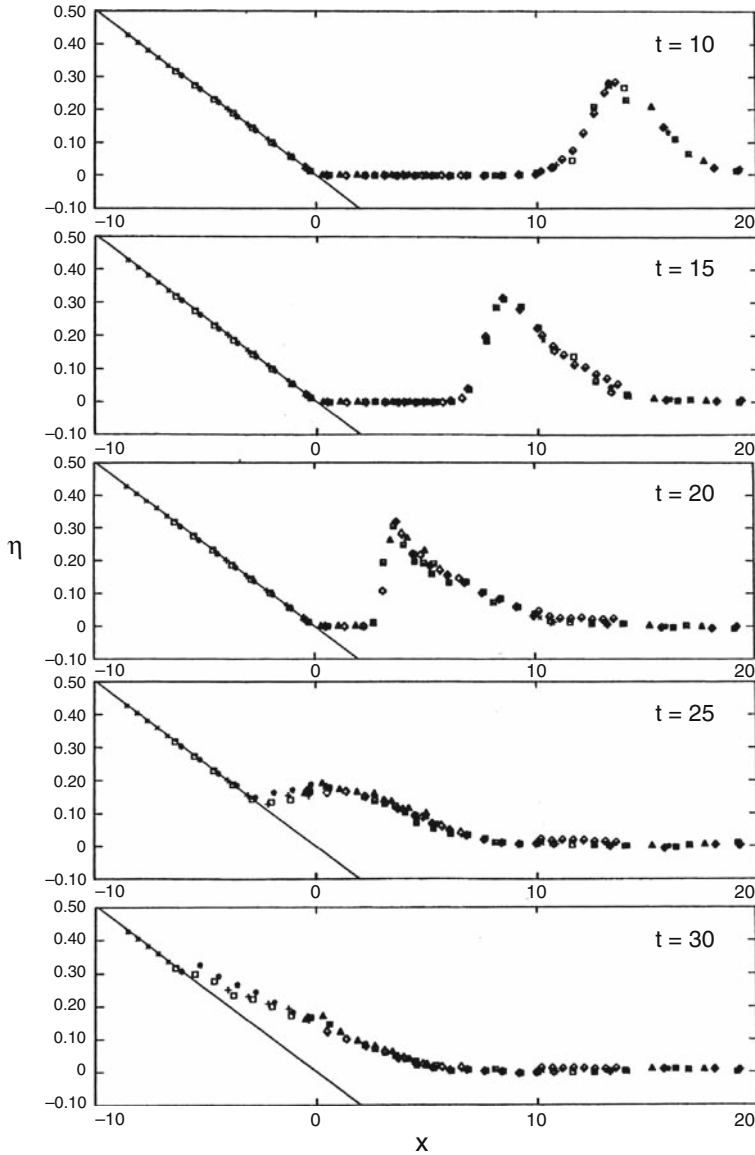
Figure 11

Time evolution of a $\tilde{H}/\tilde{d} = 0.30$ solitary wave up a 1:19.85 beach (Fig. 1). The markers show different realizations of the same experiment of SYNOLAKIS (1986). Refer to SYNOLAKIS (1986; 1987) for details.

In the physical model, a 62.5-cm-high, 7.2-m toe-diameter, and 2.2-m crest-diameter circular island with a 1:4 slope was located in the basin. Experiments were conducted at 32 cm and 42 cm water depths. Each experiment was repeated at least twice. The wavemaker trajectories were recorded to allow the assignment of the same boundary
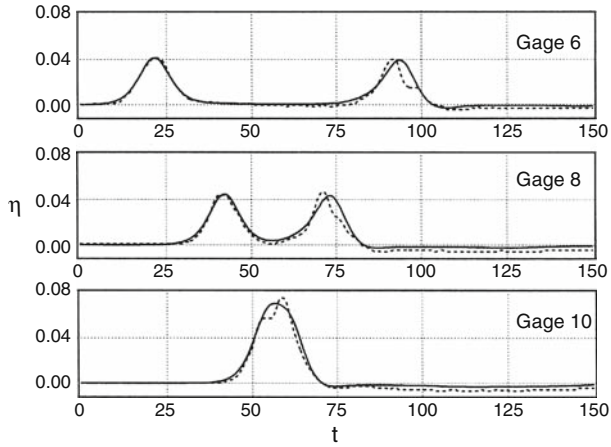
Figure 12
Comparison of the time histories of the free surface elevations midway in each sloping segment for the analytical solution (solid line) of KÂNOĞLU and SYNOLAKIS (1998) and the laboratory data (dotted line) for a $\tilde{H}/\tilde{d} = 0.038$, $\tilde{d} = 21.8$ cm, solitary wave. Refer to KÂNOĞLU and SYNOLAKIS (1998) for details.
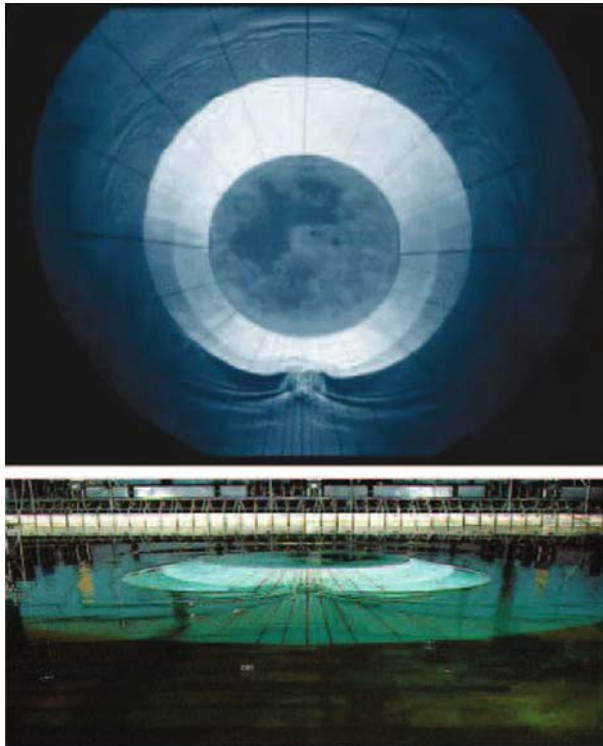

Figure 13
Views of the conical island (top) and the basin (bottom). After KÂNOĞLU and SYNOLAKIS (1998).
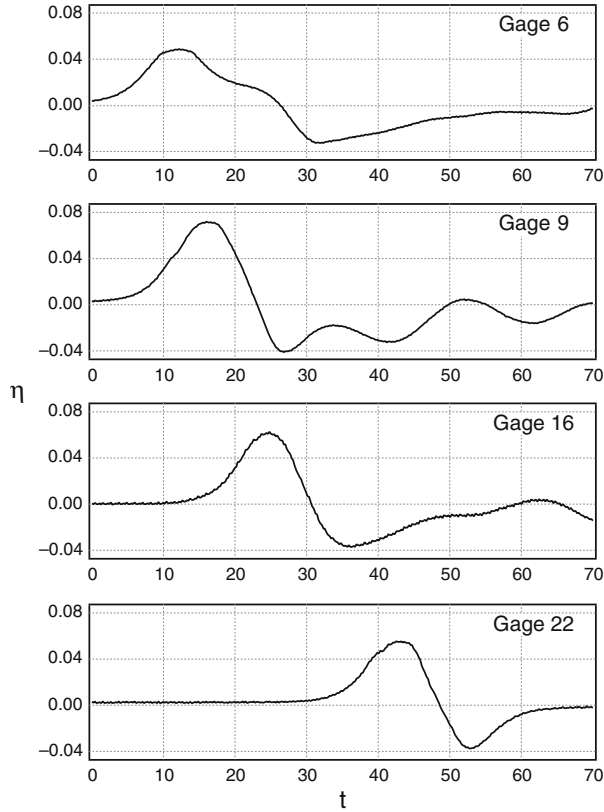
Figure 14

Laboratory data for the time histories of surface elevation for a $\tilde{H}/\tilde{d} = 0.045$, $\tilde{d} = 32$ cm, solitary wave at four gages. Gage 6 is located at the toe of the conical island on the 0° radial line, i.e., incoming wave direction. Gages 9, 16, and 22 are the gages closest to the shoreline on the 0°, 90°, and 180° radial lines respectively. Refer to LIU et al. (1995) and KÂNOĞLU and SYNOLAKIS (1998) for experimental details.

motion in numerical computations. Water-surface time histories were measured with 27 wave gages located around the perimeter of the island. One example is provided here and time histories of the surface elevation around the circular island are given at four locations (Fig. 14). Maximum runup heights around the perimeter of the island were measured at 24 locations (Fig. 15). Any numerical computation of two-dimensional runup should stably model two wave fronts that split in front of the island and collide behind it.

The conical island experiments provided runup observations for validating numerical models and supplemented comparisons with analytical results (KÂNOĞLU and SYNOLAKIS, 1998). The experiments are described in greater detail in LIU et al., 1995; BRIGGS et al., 1995; KÂNOĞLU, 1998; KÂNOĞLU and SYNOLAKIS, 1998.

Complex three-dimensional runup on a cove; Monai Valley: 2+1 numerical computations should also be benchmarked with the laboratory model of Monai Valley,
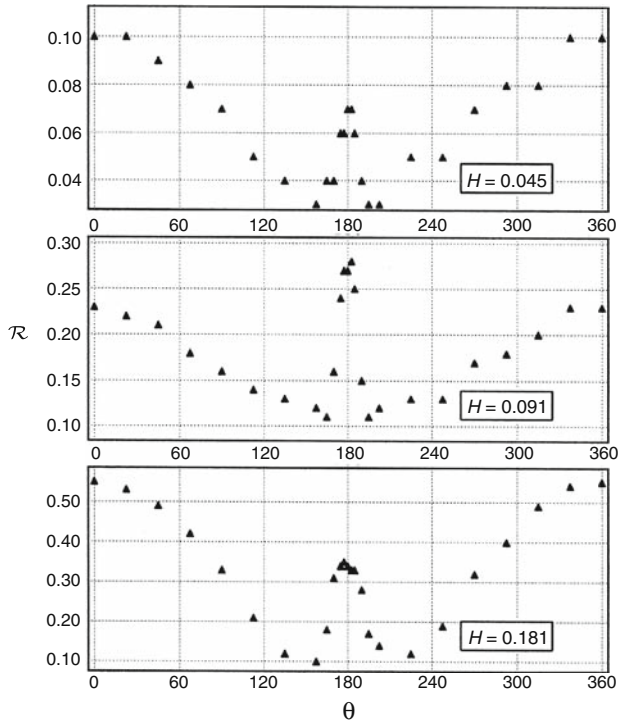
Figure 15

Maximum runup heights from the laboratory data for three solitary waves $\tilde{H}/\tilde{d} = 0.045$, 0.091, and 0.181, $\tilde{d} = 32$ cm.

Okushiri Island, Japan. The Hokkaido–Nansei–Oki (HNO) tsunami of 1993 struck Okushiri resulting in 30 m extreme runup heights and currents of the order of 10–18 m/ sec, (HOKKAIDO TSUNAMI SURVEY GROUP, 1993). The extreme tsunami runup mark was discovered at the tip of a very narrow gulley within a small cove at Monai. High resolution seafloor bathymetry existed before the event and, when coupled with bathymetric surveys following it, allowed meaningful characterization of the seafloor deformation that triggered the tsunami.

A 1/400 laboratory model closely resembles the actual bathymetry and topography of Monai Valley and was constructed in a 205-m-long, 6-m-deep, and 3.5-m-wide tank at the Central Research Institute for Electric Power Industry (CRIEPI) in Abiko, Japan (Fig. 16a). The incident wave from offshore was an LDN with a −2.5 cm leading-depression and a 1.6 cm crest following it (Fig. 16b). The vertical sidewalls were totally reflective. Waves were measured at 13 locations, as shown in Figure 16c for one location. Comparing model output for this benchmark with the laboratory data shows how well a given code performs in a rapid sequence of withdrawal and runup.

Three-dimensional landslide: Landslide wave generation remains the frontier of numerical modeling, particularly for subaerial slides. The latter not only involves the
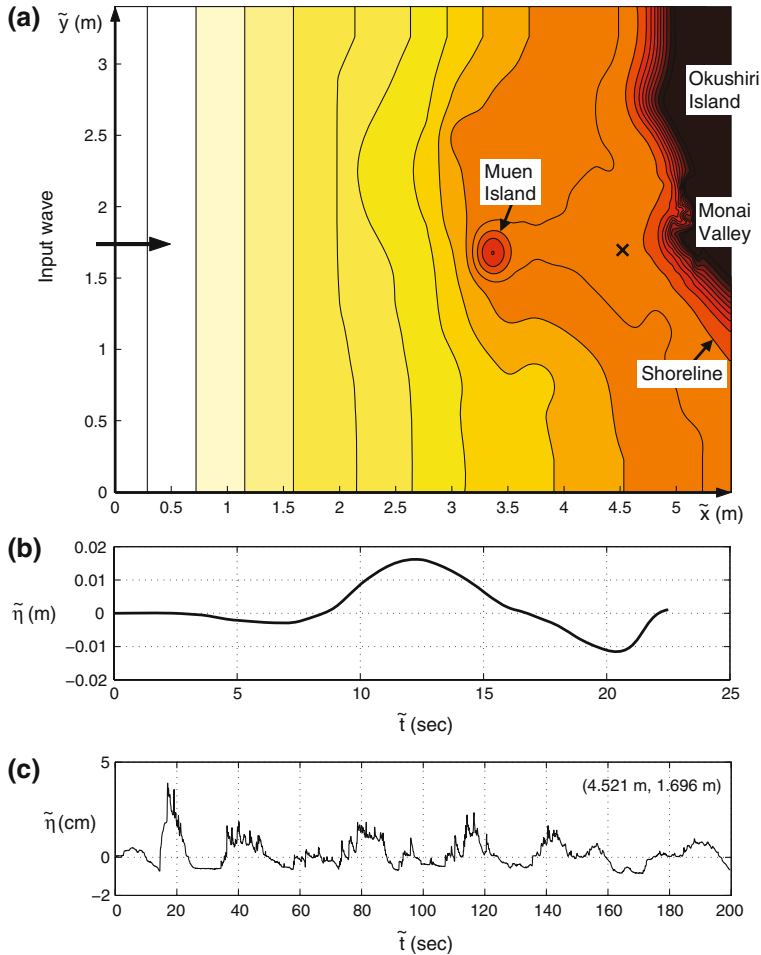
Figure 16
(a) Bathymetric and topographic profile for the Monai Valley experimental setup. Light to dark shading shows deep to shallow depth. Not to scale. (b) Input wave profile. (c) Time series of surface elevation at (4.521 m, 1.696 m).

rapid change of the seafloor, but also the impact with the still water surface. Numerical codes that will be used to model subaerial-landslide triggered tsunamis need to be tested against three-dimensional landslide benchmarks.

Large-scale experiments have been conducted in a wave tank with a 104-m-long, 3.7-m-wide, and 4.6-m-deep wave channel with a plane slope (1:2) located at one end of the tank; part of the experimental setup is shown in Figure 17, after RAICHLEN and SYNOLAKIS (2003). A solid wedge was used to model the landslide. The triangular face had a horizontal length of 91 cm, a vertical face with a height of 45.5 cm, and a width of 61 cm (Fig. 17). The horizontal surface of the wedge was initially positioned either a short
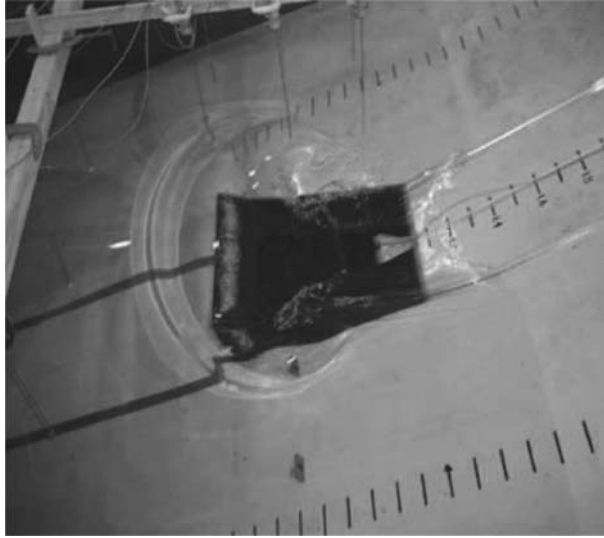
Figure 17
A picture of part of the experimental setup. After RAICHLEN and SYNOLAKIS (2003).
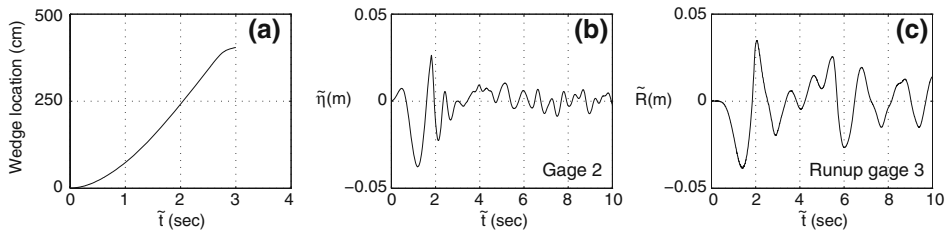

Figure 18
(a) Time histories of the block motion, (b) time histories of the surface elevation, and (c) runup measurements for the submerged case with $\Delta = -0.1$ m. Gage 2 and runup gage 3 are located approximately one wedge-width away from the center cross-section, i.e., 0.635 m and 0.61 m, respectively. While gage 2 is located 1.245 m away from the shoreline, the runup gage 3 is located at the shoreline. Refer to LIU *et al.* (2005) for details.

distance above or below the still water level to reproduce a subaerial or submarine landslide. The block was released from rest, abruptly moving downslope under gravity, rolling on specially designed wheels (with low friction bearings) riding on aluminum strips with shallow grooves inset into the slope. The wedge was instrumented with an accelerometer to measure the acceleration-time history and a position indicator to independently determine the velocity and position time histories which can be used for numerical modeling (Fig. 18).

A sufficient number of wave gages were used to determine the seaward propagating waves, the waves propagating to either side of the wedge, and for the submerged case, the

water surface-time history over the wedge. In addition, the time history of the runup on the slope was accurately measured. Time histories of the surface elevations and runup measurements for the case with submergence $\Delta = -0.1$ m are presented in Figure 18. A total of more than 50 experiments with moving wedges, hemispheres, and paralleliped bodies were conducted, and the wedge experiments were used as benchmark tests in the 2004 Catalina Island, Los Angeles, California workshop (LIU *et al.*, 2008). Details and more experimental results can be found in RAICHLEN and SYNOLAKIS (2003) and LIU *et al.* (2005).

2.2.3 Field data benchmarking. Verification of any model in a real-world setting is essential, after all computations are presumed to model geophysical reality, especially for operational models. Benchmark testing is a necessary but not a sufficient condition. The main challenge of testing a model against real-world geophysical data is to overcome the uncertainties inherent in the definition of the tsunami source. While the source of the wave is deterministic in the controlled setting of the laboratory experiment and can usually be reproduced with precision in computations, the initialization of the numerical computation of a prototype tsunami is not as well constrained. It has not been uncommon for modelers to introduce ad hoc amplification factors in standard source solutions a la OKADA (1985) to obtain better agreement between their runup predictions and observations. Clearly such comparisons are circuitous, and fortunately with the further deployment of DART buoys—tsunamographs—they will be obsolete. For tsunamis, deep-ocean measurements (BERNARD *et al.*, 2006) are the most unambiguous data quantifying the source of a tsunami. One example of tsunami source quantification through deep-ocean measurements is given in WEI *et al.* (2008).

No DART buoys—tsunameters—existed in the Indian Ocean at the time of the megatsunami, since DART buoys then had only been deployed in the Pacific Ocean. Satellite altimetry measurements of the Indian Ocean tsunami provide insufficient quality and coverage to constrain the tsunami source. Hydrodynamic inversion remains an ill-posed problem and criteria for its regularization are lacking. Hence, the 2004 event is not as yet one of the better operational benchmarks in terms of forecasting inundation, given the still raging debate as to the details of the seafloor deformation.

Deep-ocean measurements allow for more defensible inversions, since they are not affected by local coastal effects. Several events have been recorded by both deep-ocean and coastal gages in the Pacific and allow reasonably constrained comparison with models. The expanded DART system array will be providing more tsunami measurements for future events, expanding the library of well-constrained propagation scenarios for model verification. NOAA's National Geophysical Data Center (http://www.ngdc.noaa.gov/hazard/tsu.shtml), NOAA's Tsunami Warning Centers (http://www.prh.noaa.gov/ptwc/ and http://wcatwc.arh.noaa.gov/), and NOAA's Center for Tsunami Research (http://nctr.pmel.noaa.gov/) websites provide updated information on the latest tsunami data. Here, we first present field data for the 1993 HNO tsunami then
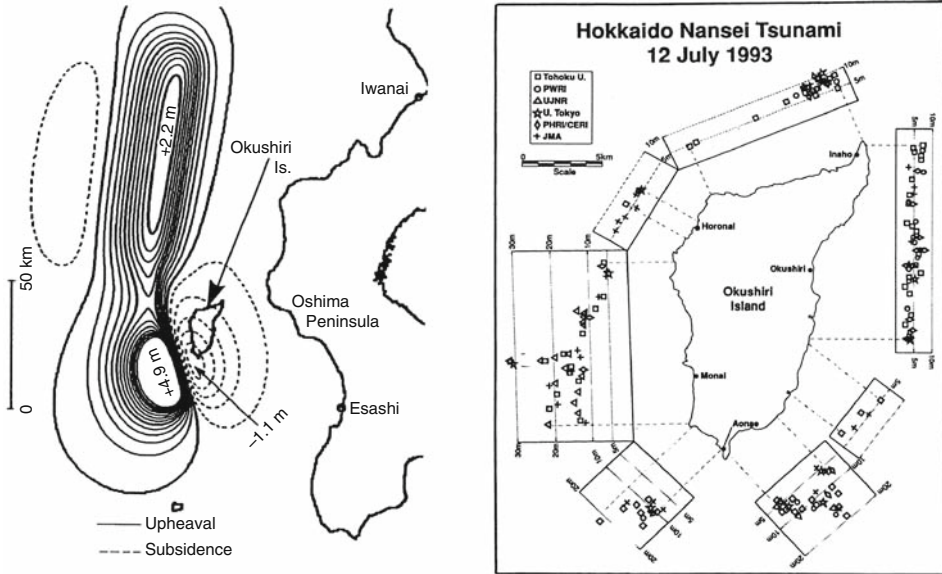
Figure 19
(Left inset) Fault plane constructed by the Disaster Control Research Center, Japan. (Right inset) Maximum runup measurements around Okushiri Island. Refer to TAKAHASHI (1996) for details.

present the data used for the first real-time model forecast test as an example of data which might be used for model verification.

Okushiri Island: 2+1 numerical computations should be tested with the field runup measurements from the HNO tsunami around Okushiri, Japan. The bathymetry data set and the initial condition formulated a benchmark problem for the 2nd International Long-Wave Runup Models Workshop and are thoroughly explained in TAKAHASHI (1996). The magnitude $M_s = 7.8$ HNO earthquake occurred on 12 July, 1993 with a depth of 37 km hypocenter located off the southwestern coast of Hokkaido. There are several field observations which need to be explained by numerical modeling. First, the computation should estimate the wave arrival at Aonae 5 min after the earthquake. The numerical model should generate two waves at Aonae approximately 10 min apart; with the first wave arriving from the west and the second from the east. In addition, the tide gage records as presented in TAKAHASHI (1996) need to be estimated. Maximum runup predictions should then be compared with the measurements (Fig. 19). The runup high at Hamatsumae, east of Aonae needs to be illustrated, as the locale is sheltered against the direct attack of the tsunami by Aonae point.

The Rat Islands tsunami: For operational codes, benchmark testing should invert the tsunameter signal of the 17 November, 2003 Rat Islands tsunami to improve the initial estimate of sea-surface displacement derived from a seismic deformation model. It should then use the results as input to a Hilo, Hawaii inundation model to hindcast the tide gage
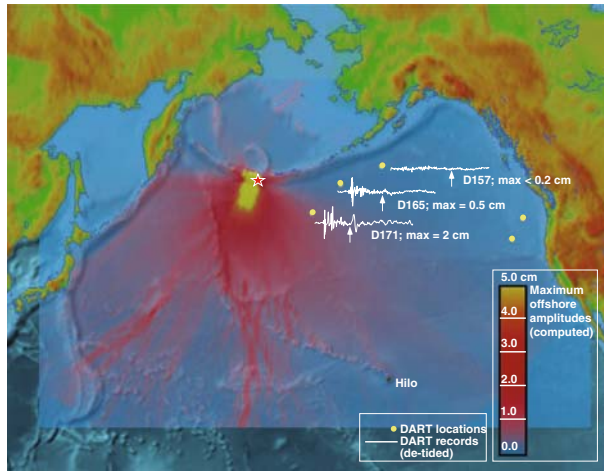
Figure 20
Propagation of the 17 November, 2003 Rat Islands tsunami. Star indicates epicenter location of the earthquake. Yellow dots are locations of DART buoys. White lines near the DART locations show recorded tsunami signal (detided) at corresponding tsunameter, arrows indicate tsunami arrival on the recordings. Filled colors show example of computed maximum tsunami amplitudes of a model propagation scenario.

record observed during the tsunami at Hilo. This is the most difficult but most realistic test for any operational model, for it involves a forecast (now hindcast) and needs to be done much faster than real time.

The magnitude $M_w = 7.8$ parent earthquake was located near Rat Islands, Alaska. This tsunami was detected by three tsunameters located along the Aleutian Trench and was also recorded at many coastal locations (TITOV et al., 2005). The combined use of tsunami propagation and inundation models is required for simulation of tsunami dynamics from generation to inundation. The test requires matching the propagation model data with the DART recording to constrain the tsunami source model (Fig. 20). If a finite-difference method on a structured grid is used, several nested numerical grids would allow *telescoping* from a coarse-resolution propagation model into a high-resolution inundation model with a model grid of at least 50 m resolution. If an unstructured grid method is used, a single grid may include enough resolution near the coast. The data-constrained propagation model should drive a high-resolution inundation model of Hilo Harbor. The inundation model being tested should reproduce the tide gage record at Hilo (Fig. 21). Since this benchmarking is required for the forecasting models, it is essential to model four hours of Hilo Harbor tsunami dynamics in 10 min of computational time.

2.3. Scientific Evaluation

Peer-review documentation: Any model used for inundation mappings or operational forecasts must be published in peer-reviewed scientific journals. One or more of these
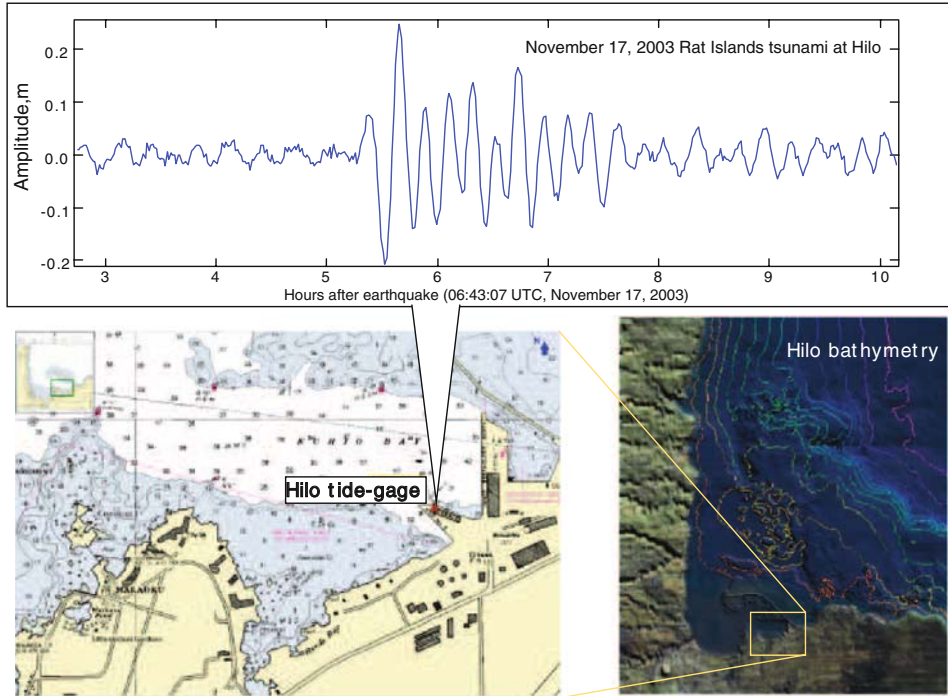
Figure 21
Location of Hilo tide gage and the recording of the 17 November, 2003 Rat Islands tsunami.

publications should include either the benchmark comparisons described here or their equivalents. However, it must be stressed that a single comparison is not sufficient.

Formal scientific evaluation: To identify best available practices and set standards based on these practices, a formal evaluation process of individual models needs to be established. This process may include solicitation of additional reviews of the model's veracity by experts.

2.4. Operational Evaluation

To ensure consistency in interpretation, the same model(s) should be used to produce inundation map and operational forecast products. If a tsunami inundation model is under consideration to generate operational forecast products, then an additional evaluation should be conducted to determine the suitability of the model for operational applications. This evaluation should be conducted in a test-bed environment consisting of research and operational parts, in order to assess a number of model features that bear on important operational factors, such as special implementation hardware/software issues, ease of use, computation time, etc. In particular, the operational evaluation of

candidate models for real-time forecasting and inundation mapping should include the following steps:

Step 1—*Meet operational forecasting and inundation mapping requirements and objectives*: Operational requirements include: Basic forecasting and inundation computation; analysis and visualization tools; integration with operations (vs. separate, stand-alone applications); basic data assimilation techniques; computational resources needed to meet milestones; etc. If a candidate model does not meet specified forecasting or inundation mapping requirements and objectives, it should be rejected at this point.

Step 2—*Meet modular development requirements*: Various pieces of the forecast model must be developed in parallel, based on the overall objectives defined in step 1.

Step 3—*Meet test bed and model standards*: In this step, the candidate model is tested against operational standards, with special attention given to its ability to simulate previous major tsunamis with the required speed and accuracy. Based on these test results, forecast model development may return to step 2, proceed, or the candidate model may be rejected for operational use.

Step 4—*Meet operational testing requirements*: The candidate model is integrated into the operational setting for testing. Potential sources are defined and the model is tested in a forecasting mode on an operational platform. Graphical interfaces are developed and forecast models are applied to a few cases to test operational integration and important individual factors such as speed, accuracy, and reliability (see section 3). Operational testing and feedback is provided by the TWCs at this point, and adjustments are made as necessary.

Step 5—*Implement operationally*: The model is fully integrated into the operational setting and procedures.

3. Criteria for Evaluating Operational Forecasting and Inundation Mapping Models

Given the accumulated experience in the tsunami community in the past 50 years, it is now possible to describe the requirements for an ideal tsunami model. Given an earthquake fault mechanism and tsunameter data, the ideal model should satisfactorily predict tsunami inundation at-risk coastlines in a sufficiently short time. Sufficiently short is defined as any time interval between the initiation of the tsunami and the calculation of the inundation forecast that allows for evacuation of the target communities. For example, the State of Hawaii needs about three hours for a complete and orderly evacuation. An ideal model would accurately forecast inundation at least three hours before the tsunami impact is expected anywhere in Hawaii.

3.1. Model Computational Time Constraints

Computational speed standards for inundation mapping and real-time forecasting are different. Inundation mapping can safely be conducted over months. An effective

short-term forecast must be produced faster than real-time. It should be available a few minutes before the tsunami strikes the nearest community, to allow sirens to trigger the evacuation of beach and coastal residents and give emergency personnel time to mobilize resources and prepare for search and rescue. Furthermore, a forecast must correctly predict the duration of the series of waves that comprise the tsunami event, to identify when it will be safe for search and rescue operations to begin without endangering the lives of responders. Tsunamis often became trapped in closed bays or on the continental shelf, resulting in sea-level oscillations that may persist for several hours. During the 1993 HNO tsunami, bay oscillation at Aonae trapped the tsunami for over 30 min, and a large portion of Aonae remained submerged for much of this time. The Crescent City, California harbor oscillated for several hours following the 15 November, 2006 tsunami (USLU *et al.*, 2007).

3.2. *Model Accuracy Constraints*

The accuracy of any given model depends on how well the computational procedure represents the correct solution of the parent equations of motion. When exact solutions exist (as, for example, for certain cases of the LSW and NSW equations), the determination of the accuracy of a solution algorithm is straightforward, i.e., through comparisons of the numerical results with the analytical predictions. Determining maximum runup numerically within 5% of the analytical solution is now possible with a handful of models.

For most bathymetries of geophysical interest, analytical solutions do not exist, and it is unlikely that they will ever be determined, due to the complexity of the physical terrain. However, a few laboratory models at smaller scale than the prototype exist. The Catalina Island, Los Angeles, 2004 model validation workshop of the National Science Foundation identified a handful of models that could predict the laboratory measurements within 10%. While greater compliance with measurements is hoped for in the next decade, 10% accuracy with respect to laboratory experiments is achievable now and should be considered a standard. In addition, for operational forecast models, propagation accuracy of 10% and an error in estimating arrival times for farfield events of 3 min, both are now possible (TITOV *et al.*, 2005).

An associated accuracy constraint is grid resolution. This depends on the complexity of the shoreline. On a fairly plane, wide, and very long beach such as those of Southern California, a 100-m-grid resolution may be sufficient. The smallest offshore and onshore features likely to affect tsunami impact on a coastal community should be reflected in the numerical grids. If a community is fronted by a sand spit of width 100 m, at least four grid points are needed to provide accurate resolution of the flow over the spit.

We emphasize again that laboratory and analytical benchmarks are necessary but not sufficient conditions for confidence for extrapolation of the methodology at geophysical scales. One example is wave-breaking. While a numerical model may realistically approximate the solution of the Navier–Stokes equations at laboratory scales, it may not do

so at large scales. Calculating the evolution of breaking waves involves calculating turbulent shear terms and invoking turbulence closure constraints which are scale-dependent. Therefore a reliability constraint needs to be applied, and this is discussed next.

3.3. Model Reliability and Reality Constraints

Model reliability refers to how well a given model predicts inundation consistently and realistically at geophysical scales. Linear theory may predict wave evolution consistently, but not always realistically. For example, linear theory predicts that the height of shoaling waves will grow continuously; in reality, however, waves will eventually break, if they exceed threshold height-to-depth and height-to-wavelength ratios.

Reliability is a crucial issue. Several widely-used numerical models include *ad hoc* friction factors. These factors were not developed to model the physical manifestation of frictional dissipation but to stabilize what is by its very nature a marginally stable computation. It is therefore not possible to know *a priori* how well a model that has been fairly successful in a small number of cases performs in general. For example, a model developed and calibrated to provide stable computations along steep coastlines for which inundation distances are less than 200 m may not perform equally well when forecasting inundation penetration of more than 3 km inland, as in the case of Banda Aceh during the 26 December, 2004 Boxing Day tsunami.

Clearly, any numerical model must be tested over a variety of scales from the laboratory to prototype to ensure both reliability and realism. Ideally, inundation models should be continuously tested with every new set of laboratory data or tsunami field data that becomes available. This will also allow for their further improvement.

4. Conclusions

State-of-the-art inundation codes in use today have evolved through a painstaking process of careful validation and verification. Operational forecast models based on these codes have been developed through extensive additional verification with measurements from real tsunamis. Mining this experience, procedures for approval and application of numerical models for operational uses are proposed as: establishment of standards for model validation and verification; scientific evaluation of individual models; operational evaluation of individual models; development of operational applications for forecasting; and procedures for transfer of technology to operations. Only through parallel testing of models under identical conditions, as when there is a tsunami emergency and an operational forecast is performed, can the community determine the relative merits of different computational formulations, an important step to further improvements in speed, accuracy, and reliability.

NOAA has adopted the standards and procedures discussed here for the development and evaluation of operational models for the Pacific and the West Coast/Alaska TWCs

(Synolakis *et al.*, 2007; http://nctr.pmel.noaa.gov/benchmark/). In addition to NOAA, UNESCO's Intergovernmental Coordination Group (ICG) for the Indian Ocean Tsunami Warning and Mitigation System (ICG/IOTWS) adapted a similar document based on Synolakis *et al.* (2007) during its fourth session at Mombasa, Kenya on 28 February–2 March, 2007 with additional field benchmarking for Sumatra, 26 December, 2004; Nias, 28 March, 2005; Tonga, 3 May, 2006; and Java, 17 July, 2006 events. Also, again UNESCOs ICG for the Northeastern Atlantic, the Mediterranean and Connected Seas Tsunami Early Warning and Mitigation System (ICG/NEAMTWS) is considering adoption of a similar document as well.

It is again emphasized that model testing must be a continuous process. Operational products produced in real time during an actual event must be thoroughly reviewed, and the operational models must be systematically tested in hindcast mode after each tsunami strike. The results must be documented and reported to the community in order to develop and implement improvement through the identification and resolution of any serious problems or inadequacies of the models and/or products. While this process may appear onerous, it does reflect our current state of scientific knowledge. This process is thus the only defensible methodology when human lives are at stake.

Acknowledgements

REFERENCES

Associated Press (2005), *New analysis boosts potential tsunami threat*, December 7, 2005. http://www.kgw.com/sharedcontent/APStories/stories/D8EBN7NO7.html.

Bernard, E.N., Mofjeld, H.O., Titov, V., Synolakis, C.E., and González, F.I. (2006), *Tsunami: Scientific frontiers, mitigation, forecasting, and policy implications*, Philos. T. R. Soc. A *364*, 1989–2007.

Borerro, J., Ortiz, M., Titov, V.V., and Synolakis, C.E. (1997), *Field survey of Mexican tsunami*, EOS Trans. Amer. Geophys. Un. *78*(8), 85, 87–88 (Cover article).

Briggs, M.J., Synolakis, C.E., Harkins, G.S., and Green, D. (1995), *Laboratory experiments of tsunami runup on a circular island*, Pure Appl. Geophys. *144*, 569–593.

Carrier, G.F. and Greenspan, H.P. (1958), *Water waves of finite amplitude on a sloping beach*, J. Fluid Mech. *17*, 97–110.

Carrier, G.F., Wu, T.T., and Yeh, H. (2003), *Tsunami runup and drawdown on a sloping beach*, J. Fluid Mech. *475*, 79–99.

ETHNOS (2007), *Predictions for earthquakes and tsunamis*, http://www.ethnos.gr/article.asp?catid=11386&subid=2&pubid=139228.

GORING, D.G. (1978), *Tsunamis—the propagation of long waves onto a shelf*, W.M. Keck Laboratory of Hydraulics and Water Resources, California Institute of Technology, Pasadena, California. Report No. KH-R-38.

GRILLI, S.T., SVENDEN, I.A., and SUBRAYAMA, R. (1997), *Breaking criterion and characteristics of solitary waves on a slope*, J. Waterw. Port Coast. Ocean Eng. *123*(2), 102–112.

HALL, J.V. and WATTS, J.W. (1953), *Laboratory investigation of the vertical rise of solitary waves on impermeable slopes*, Tech. Memo. 33, Beach Erosion Board, U.S. Army Corps of Engineers, 14 pp.

HAMMACK, J.L. (1972), *Tsunamis—A model for their generation and propagation*, W.M. Keck Laboratory of Hydraulics and Water Resources, California Institute of Technology, Pasadena, California, Report No. KH-R-28.

HOKKAIDO TSUNAMI SURVEY GROUP (1993), *Tsunami devastates Japanese coastal region*, EOS Trans. Amer. Geophys. Un. *74*(37), 417 and 432.

KÂNOĞLU, U. (1998), *The runup of long waves around piecewise linear bathymetries*, Ph.D. Thesis, University of Southern California, Los Angeles, California, 90089–2531, 273 pp.

KÂNOĞLU, U. (2004), *Nonlinear evolution and runup–rundown of long waves over a sloping beach*, J. Fluid Mech. *513*, 363–372.

KÂNOĞLU, U. and SYNOLAKIS, C.E. (1998), *Long wave runup on piecewise linear topographies* J. Fluid Mech. *374*, 1–28.

KÂNOĞLU, U. and SYNOLAKIS, C. (2006), *Initial value problem solution of nonlinear shallow water-wave equations*, Phys. Rev. Lett. *97*, 148501.

KELLER, J.B. and KELLER, H.B. (1964), *Water wave runup on a beach*, ONR Research Report NONR-3828(00), Department of the Navy, Washington DC, 40 pp.

LI, Y. and RAICHLEN, F. (2000), *Energy balance model for breaking solitary wave runup*, J. Waterw. Port Coast. Ocean Eng. *129*(2), 47–49.

LI, Y. and RAICHLEN, F. (2001), *Solitary wave runup on plane slopes*, J. Waterw. Port Coast. Ocean Eng. *127*(1), 33–44.

LI, Y. and RAICHLEN, F. (2002), *Non-breaking and breaking solitary runup*, J. Fluid Mech. *456*, 295–318.

LIU, P.L.-F., CHO, Y.-S., BRIGGS, M.J., KÂNOĞLU, U., and SYNOLAKIS, C.E. (1995), *Runup of solitary waves on a circular island*, J. Fluid Mech. *320*, 259–285.

LIU, P.L.-F., LYNETT, P., and SYNOLAKIS, C.E. (2003), *Analytical solutions for forced long waves on a sloping beach*, J. Fluid Mech. *478*, 101–109.

LIU, P.L.-F., WU, T.-R., RAICHLEN, F., SYNOLAKIS, C.E., and Borrero, J. (2005), *Runup and rundown generated by three-dimensional sliding masses*, J. Fluid Mech. *536*, 107–144.

LIU, P.L.-F., YEH, H., and SYNOLAKIS, C. (eds.), *Advanced Numerical Models for Simulating Tsunami Waves and Runup*, In *Advances in Coastal and Ocean Engineering 10* (World Scientific, Singapore 2008).

MEI, C. C., *The Applied Dynamics of Ocean Surface Waves* (Wiley, New York, NY 1983).

NATIONAL SCIENCE and TECHNOLOGY COUNCIL (2005), *Tsunami Risk Reduction for the United States: A Framework for Action*, A joint report of the subcommittee on Disaster Reduction and the United States Group on Earth Observations, 30 pp.

NEW SCIENTIST (2005), *Heaving seabed triggered Asian tsunami*, December 10, 2005. http://seattletimes.nwsource.com/html/localnews/2002668973_tsunami07m.html.

OKADA, Y. (1985), *Surface deformation due to shear and tensile faults in a half-space*, Bull. Seismol. Soc. Am. *75*, 1135–1154.

PEDERSEN, G., *A Lagrangian model applied to runup problems*. In *Advanced Numerical Models for Simulating Tsunami Waves and Runup* (eds. Liu, P.L.-F., Yeh, H., and SYNOLAKIS, C.), In *Advances in Coastal and Ocean Engineering 10* (World Scientific, Singapore 2008).

PEDERSEN, G. and GJEVIK, B. (1983), *Runup of solitary waves*, J. Fluid Mech. *135*, 283–299.

RAICHLEN, F. and SYNOLAKIS, C.E. (2003), *Runup from three- dimensional sliding masses*, Proc. *Long Waves Symposium*, Thessaloniki, Greece (eds. M. Briggs, and Ch. Koutitas), pp. 247–256.

SATAKE, K., OKAL, E.A. and BORRERO, J.C. (2007), *Tsunami and its hazard in the Indian and Pacific Oceans: Introduction*, Pure Appl. Geophys. *164*(2-3), 249-259.

SHUTO, N. (1973), *Shoaling and deformation of nonlinear waves*, Coastal Eng. Japan *16*, 1–12.

SYNOLAKIS, C.E. (1986), *The Runup of Long Waves*, Ph.D. Thesis, California Institute of Technology, Pasadena, California, 91125, 228 pp.

SYNOLAKIS, C.E. (1987), *The runup of solitary waves*, J. Fluid Mech. *185*, 523–545.

SYNOLAKIS, C.E. (1991), *Green law and the evolution of solitary waves*, Phys. Fluids A-Fluid Dynamics *3*, 490-491.

SYNOLAKIS, C.E. and SKJELBREIA, J.E. (1993), *Evolution of maximum amplitude of solitary waves on plane beaches*, J. Waterw. Port Coast. Ocean Eng. *119*(3) 323–342.

SYNOLAKIS, C.E. and OKAL, E.A. (2005), *1992–2002: Perspective on a decade of post-tsunami surveys*, Adv. Nat. Technol. Hazards *23*, 1-30.

SYNOLAKIS, C.E. and BERNARD, E.N. (2006), *Tsunami science before and after Boxing Day 2004*, Phil. Trans. R. Soc. A *364*(1845), 2231–2265.

SYNOLAKIS, C.E. and KONG, L. (2006), *Runup measurements of the December 2004 Indian Ocean Tsunami*, Earthq. Spectra *22* (Suppl. 3), S67-S91.

SYNOLAKIS, C.E., BERNARD, E.N., TITOV, V.V., KÂNOĞLU, U., and GONZÁLEZ, F. (2007), Standards, criteria, and procedures for NOAA evaluation of tsunami numerical models. NOAA OAR Special Report, Contribution No 3053, NOAA/OAR/PMEL, Seattle, Washington, 55 pp.

TADEPALLI, S. and SYNOLAKIS, C.E. (1994), T*he runup of N-waves on sloping beaches*, Proc. R. Soc. Lond. A. *445*, 99–112.

TADEPALLI, S. and SYNOLAKIS, C.E. (1996), *Model for the leading waves of tsunamis*, Phys. Rev. Lett. *77*(10), 2141–2144.

TAKAHASHI, T., *Benchmark problem 4; the 1993 Okushiri tsunami—Data, conditions and phenomena*. In *Long-Wave Runup Models* (eds. Yeh, H., Liu, P.L.-F., and SYNOLAKIS, C.E.) (World Scientific Publishing, Singapore 1996) pp 384–403.

THE SEATTLE TIMES (2005), *Tsunami expers forecast raises a flag*, December 7, 2005, http://seattle-times.nwsource.com/html/localnews/2002668973_tsunami07m.html.

TITOV, V.V. and SYNOLAKIS, C.E. (1995), *Modeling of breaking and nonbreaking long-wave evolution and runup using VTCS-2*, J. Waterw. Port Ocean Coast. Eng. *121*(6), 308–316.

TITOV, V.V. and GONZÁLEZ, F.I. (1997), *Implementation and testing of the method of splitting tsunami (MOST)*, NOAA Technical Memorandum ERL-PMEL-112, PB98-122773, Pacific Marine Environmental Laboratory, Seattle, Washington, 11 pp.

TITOV, V.V. and SYNOLAKIS, C.E. (1997), E*xtreme inundation flows during the Hokkaido–Nansei–Oki tsunami*, Geophys. Res. Lett. *24*(11), 1315–1318.

TITOV, V.V. and SYNOLAKIS, C.E. (1998), *Numerical modeling of tidal wave runup*, J. Waterw. Port Ocean Coast. Eng. *124*(4), 157–171.

TITOV, V.V., GONZÁLEZ, F.I., BERNARD, E.N., EBLE, M.C., MOFJELD, H.O., NEWMAN, J.C., and VENTURATO, A.J. (2005), *Real-time tsunami forecasting: Challenges and solutions* Nature Hazard *35*(1), 41–58.

TUCK, E.O. and HWANG, L.S. (1972), *Long-wave generation on a sloping beach*, J. Fluid Mech. *51*, 449–461.

USLU, B., BORRERO, J.C., DENGLER, L.A., and SYNOLAKIS, C.E. (2007), *Tsunami inundation at Crescent City, California generated by earthquakes along the Cascadia Subduction Zone*, Geophys. Res. Lett. *34*, L20601.

WEI, Y., BERNARD, E.N., TANG, L., WEISS, R., TITOV, V.V., MOORE, C., SPILLANE, M., HOPKINS, M., and KÂNOĞLU, U. (2008), *Real-time experimental forecast of the Peruvian tsunami of August 2007 for U.S. coastlines*, Geophys. Res. Lett *35*, L04609.

YEH, H., LIU, P.L.-F., BRIGGS, M., and SYNOLAKIS, C.E. (1994), *Tsunami catastrophe in Babi Island*, Nature *372*, 6503–6508.

YEH, H., LIU, P.L.-F., and SYNOLAKIS, C.E. (eds.), *Long-Wave Runup Models* (World Scientific Publishing, Singapore 1996).

ZELT, J.A. (1991), *The runup of breaking and nonbreaking solitary waves*, Coastal Eng. *125*, 205–246.

To access this journal online:
www.birkhauser.ch/pageoph